



Study of methylene blue adsorption from solution by magnetic graphene oxide composites

Mingyu Liu, Jiajia Dong, Weili Wang, Mengmeng Yang, Yifan Gu, Runping Han*

College of Chemistry and Molecular Engineering, Zhengzhou University, No 100 of Kexue Road, Zhengzhou, 450001 China, Tel. +86 371 67781757; Fax: +86 371 67781556; emails: rphan67@zzu.edu.cn (R. Han), lmylittlerain@163.com (M. Liu), 792893265@qq.com (J. Dong), 1063455250@qq.com (W. Wang), 1582415059@qq.com (M. Yang), 503153641@qq.com (Y. Gu)

Received 24 October 2018; Accepted 7 January 2019

ABSTRACT

Magnetic graphene oxide (MGO) was synthesized by co-precipitation and used as an adsorbent for the removal of methylene blue (MB) from aqueous solution in batch mode. Characterizations of the materials before and after modification were performed using several techniques such as scanning electron microscopy, Fourier transform infrared spectroscopy, vibrating-sample magnetometry, Raman spectra, X-ray photoelectron spectroscopy (XPS), etc. The effects of adsorbent dose, solution pH, common salt concentrations, MB concentration, and contacting time were systematically investigated. Results showed that the adsorption capacity at 313 K could reach up to 62.7 mg·g⁻¹. The optimal pH was 9 and the salinity was disadvantageous of MB adsorption. Equilibrium adsorption data were best fitted by Koble–Corrigan model, indicating that the adsorption process may be based on multi-layer heterogeneous adsorption and controlled by chemical adsorption process. The Elovich kinetic model can be used to describe the process of MB adsorption, indicating that the adsorption process may be the diffusion process of non-homogeneous phase. Thermodynamic analyses showed that the adsorption process was spontaneous, endothermic and entropic increase. In addition, the possible adsorption mechanism was also proposed based on the experimental results and XPS analysis. It is concluded that the mechanism of MB adsorption be mainly π - π bond and electrostatic force. Furthermore, MB-loaded MGO can be reused in a secondary adsorption for removal of congo red with the adsorption capacity of 319 mg·g⁻¹. Based on the results, it was inferred that MGO could be used as a promising adsorbent for dye removal.

Keywords: Magnetic graphene oxide composites; Adsorption; Methylene blue; Congo red

1. Introduction

Water pollution caused by various dyes is one of the most ubiquitous and critical global environmental issue for people. Dyes are commonly used in the industries such as textile, leather, cosmetics, paper, food, plastics, etc. The presence at concentrations above their permissible values is highly visible and undesirable [1,2]. There are different kinds of treatment methods to decontaminate wastewater, such as biological treatment, photodegradation, hydrolysis, membrane filtration, ion exchange, and adsorption [3]. Of all the technologies

that have been proposed to remove dye contaminations, adsorption method is regarded as one of the most promising methods because of its high efficiency, convenience, and economic viability [4]. Various adsorbents have been reported to study on the removal of dyes, including biomass, clays, carbon materials [5–7]. The success of adsorption separation depends on the performance of adsorbents to a large extent. Therefore, modifying adsorbent is the primary problem in determining adsorption experiments. At present, there are various kinds of adsorbents and different uses, but the most widely used new materials are mainly carbon adsorbents and magnetic adsorbents [8].

* Corresponding author.

Graphene oxide (GO), a two-dimensional monolayer nanomaterial of sp^2 -bonded carbon atoms packed densely in a hexagonal honeycomb lattice, is considered as the most promising material because of its good mechanical properties, electrochemical and thermal properties, and large specific surface area [9]. Functionalized GO has good application prospects in molecular sensing, catalysis, photothermal therapy, energy storage, and environmental protection [10,11]. In recent years, there are more and more reports about the application of GO to remove ionic dyes from wastewater, due to the special thin graphite structure, large specific surface area with oxygen-containing functional groups such as hydroxyl, epoxy and carboxyl groups, and π - π electron system [12]. There have been reported using GO and its amine-functionalized composite to remove pollutants from aqueous solution [13]. However, GO is hard to separate from aqueous solution after adsorption, hence requires a high-speed centrifugation to achieve the separation effect, and it is unrealistic for the treatment of wastewater practically [14]. To overcome these issues, the introduction of magnetism can greatly reduce the energy consumption in the adsorption process. Magnetic materials have good dispersibility, easy functionalization and good biocompatibility. They can be applied in medicine, diagnosis, adsorption, cell biology and other related fields [15–17]. Because of its unique magnetic properties, magnetic materials can be separated from mixtures under the effect of external magnetic field, which can solve the problem that the traditional method is not easy to separate in some system. So there is a good application prospect in environmental water treatment. The preparation of graphene-based Fe_3O_4 nanocomposites have been reported recently [18,19]. However, there has been no related literature yet for the secondary adsorption of dyes from solution by magnetic graphene oxide (MGO) composites.

In this work, the introduction of iron oxide magnetic nanoparticles into GO was proposed to constitute a novel adsorbent composite, which combine the high adsorption property of GO and the separation convenience of magnetic nanoparticles. MGO was synthesized by depositing

magnetic iron oxide nanoparticles on the surface of GO nanosheets to remove methylene blue (MB), one of the cationic dyes. The interaction between MB and MGO, and the adsorption mechanism of MGO were also investigated. Adsorption kinetics and equilibrium were shown and adsorption models were applied. Furthermore, the MGO and MB-loaded MGO were then used to remove congo red (CR), an anionic dye. It was found that the secondary adsorption was also highly efficient.

2. Materials and methods

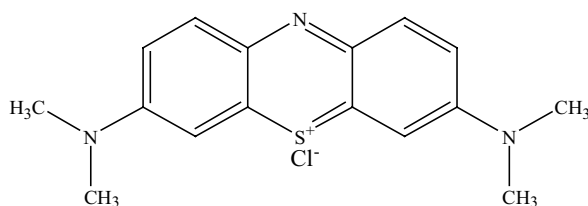
2.1. Materials

Single-layer GO powder (0.5–5 μm , Nanjing XFNANO Materials Tech. Co., Ltd., Nanjing, China), ferric chloride ($FeCl_3 \cdot 8H_2O$, Fengchuan Chemical Reagent, Tianjin, China), ferrous sulfate ($FeSO_4 \cdot 7H_2O$, Sinopharm Chemical Reagent, Shanghai, China), ammonium hydroxide (25%–28%, w/w, Sinopharm Chemical Reagent, Shanghai, China) were all purchased. The structure of MB dye (Kermel, Tianjin, China) and congo red dye (Aladdin Industrial Corporation, Shanghai, China) are shown in Fig. 1. All working solutions were prepared by diluting the stock solution with appropriate volume of distilled water. Other reagents such as HCl, NaOH, NaCl, and $CaCl_2$ were also of analytical grade.

2.2. Preparation of MGO and Fe_3O_4

The MGO composite was prepared by co-precipitation, which was similar to a method previously reported [20]. Briefly, 0.45 g GO was dissolved in distilled water under ultrasonic stirring for 1 h. Subsequently, 2.17 g of $FeSO_4 \cdot 7H_2O$ and 4.21 g of $FeCl_3 \cdot 8H_2O$ solution (molar ratio of $Fe^{2+}:Fe^{3+}$ as 1:2) were added slowly to the GO solution while stirring for 30 min. Then the temperature was raised to 65°C (water bath), and ammonia solution (28%) was added dropwise until the pH value of the solution reaches up to 11. After the reaction, the solution was aged for 30 min. Finally the

MB:



CR:

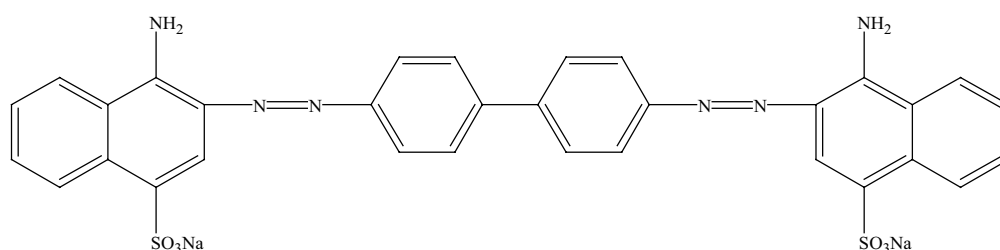


Fig. 1. Structure of MB and CR.

material was collected by magnet after being washed several times with water and ethanol until the pH was almost 7.0. Then it was dried in oven at 60°C. The obtained product was MGO. Fe₃O₄ was prepared by the same method without GO.

2.3. Characterization of GO and MGO

The pH at point zero charge (pH_{pzc}) of MGO was evaluated by the solid addition method of adjusting different pH of 10 mL 0.01 mol·L⁻¹ NaCl solution while adding 0.010 g MGO for 12 h. The pH_{initial} and pH_{final} of the solution were conducted using a pH meter (PHS-3C, China), and the pH_{pzc} is the point where pH_{initial} – pH_{final} = 0. The scanning electron microscopy (SEM, Hitachi S4800, Japan) was used to observe the morphology of the materials at an accelerating voltage of 10.0 kV. The spectra of functional groups of before and after modification were recorded in the range of 500–4,000 wave number (cm⁻¹) on the Fourier transform infrared spectroscopy (FT-IR, Nicolet iS50, USA). Raman spectra were measured by using a Raman spectroscopy (LabRAM HR Evolution, France). The magnetic properties were determined using a vibrating-sample magnetometry (VSM, Squid-VSM, USA). The analysis before and after MB adsorption were performed with X-ray photoelectron spectroscopy (XPS, ESCALAB 250Xi, England), which were further used to determine the semi-quantitative chemical composition and surface chemical states of GO and MGO.

2.4. Adsorption studies

Adsorption experiments were carried out in batch mode at 120 rpm, the adsorbents were placed in 50 mL conical flasks containing 10 mL of MB solution of various concentrations. In this study, the effect factors were as follows: the adsorbent dose (1–20 mg, C₀ = 100 mg·L⁻¹, 303 K), the initial pH (3–11) of solution (C₀ = 100 mg·L⁻¹, 303 K), co-existed ions of NaCl, CaCl₂ solution (0.005, 0.01, 0.02, 0.04, and 0.06 mol·L⁻¹, respectively, C₀ = 100 mg·L⁻¹, 303 K) and the contact time (10–720 min, C₀ = 100 mg·L⁻¹, 303 K), the adsorption temperature (293, 303, and 313 K, C₀ = 70–140 mg·L⁻¹). To investigate the reuse of MGO, the MB-loaded MGO adsorption (C₀ = 100 mg·L⁻¹, 303 K, pH = 9) was obtained. After adsorption, the MB-loaded MGO was gently washed with distilled water and dried at 333 K. For the convenience of experiment, the MGO onto CR and the secondary adsorption of the MB-loaded MGO onto CR (C₀ = 500 mg·L⁻¹, 303 K, pH = 6.06) were determined with salt and no salt.

The adsorbent and adsorbate were separated by magnetic field after adsorption, and the residual MB or CR concentration in supernatant samples was analyzed by an UV/VIS-3000 spectrophotometer (Shimadzu Brand UV-3000, Japan) of wavelengths of maximum absorbance at 664 and 499 nm, respectively. The data obtained in batch model studies were used to calculate the uptake quantity of adsorbate. The quantity of dye adsorbed onto unit weight of adsorbent (*q*, mg·g⁻¹) and the removal efficiency (*p*, %) were calculated using the following equations, respectively:

$$q = \frac{V(C_0 - C)}{m} \quad (1)$$

$$p = \frac{(C_0 - C_e)}{C_0} \times 100\% \quad (2)$$

where C₀ is the initial adsorbate concentration (mg·L⁻¹), C or C_e is the dye concentration at any time or equilibrium (mg·L⁻¹), V is the reaction solution volume (L), and m is the mass of MGO (g).

3. Results and discussion

3.1. Characterization of adsorbents

Characterization of materials can be analyzed and this is helpful to know the property of surface and explain adsorption mechanism.

3.1.1. Zero point of charge

The zero point of charge (pH_{pzc}) of materials indicate the electronic property of the functional groups on their surface and the results are shown in Fig. 2. The pH_{pzc} value of MGO was about 6.59, which meant that the material held a negatively charged surface and was likely to attract MB cationic ions when the pH was maintained above this value. And the pH_{pzc} values of the modified adsorbent moved to the acid direction, which was mainly due to the increase of the number of acidic functional groups on the surface of the adsorbent.

3.1.2. SEM of GO and MGO

The SEM images of the GO and MGO are shown in Fig. 3. As shown in Fig. 3(a), there were many wrinkles on the surface of GO and the flake two-dimensional structure increased its specific surface area. Comparing the images of GO and MGO, it could be seen clearly in Fig. 3(b) that Fe₃O₄ particles dispersed unevenly on the GO sheets, and the modification of MGO showed no significant change of the morphology of GO sheets.

3.1.3. FT-IR analysis of GO and MGO

In order to further explore the surface characteristics of GO and MGO, FT-IR analysis was performed and revealed

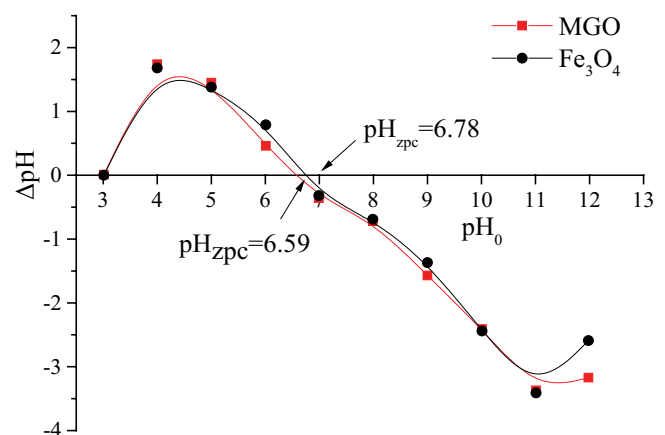


Fig. 2. Point of zero charge of Fe₃O₄ and MGO.

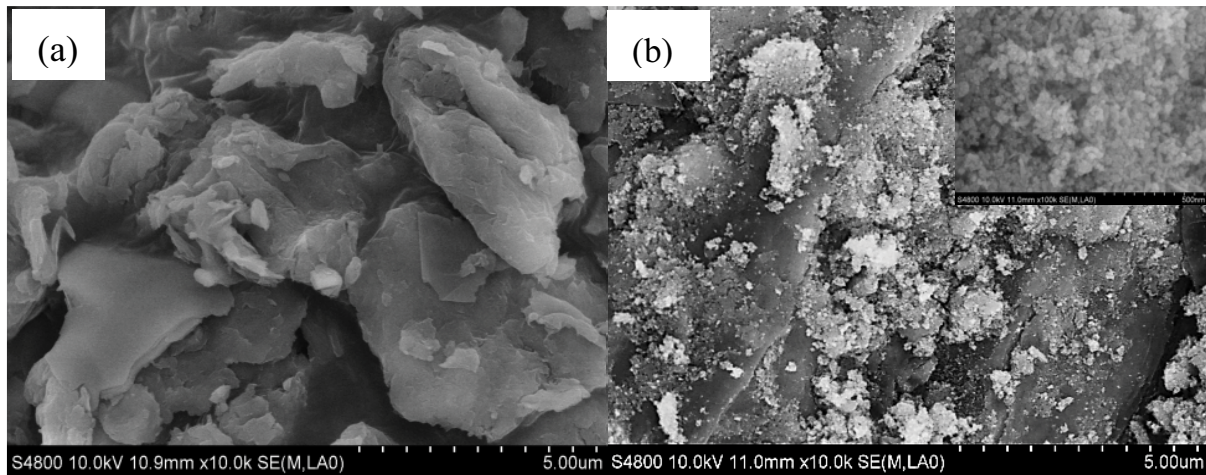


Fig. 3. SEM images of (a) GO and (b) MGO.

spectra can be seen in Fig. 4. For the spectrum of GO, the strong peak at about 3443 cm^{-1} could be caused by the stretching vibration of hydroxyl groups ($-\text{OH}$). The peak at 1630 cm^{-1} could be attributed to the $-\text{C}=\text{O}$ stretching vibration peak of carboxyl groups. The peaks from $1,000$ to $1,300\text{ cm}^{-1}$ could be associated with the $\text{C}-\text{O}-\text{C}$ stretching vibrations and $\text{C}-\text{O}$ vibration of hydroxyl groups [21].

Compared with GO, the intensities of the peaks for the oxygen-containing functional groups were weakened significantly, indicating that these groups could combine with iron groups. Magnetic materials could also conceal the peaks. And the characteristic peak of $\text{Fe}-\text{O}$ could be observed at 580 cm^{-1} , proving that Fe_3O_4 was successfully immobilized onto the GO sheets [22].

3.1.4. Raman spectra of GO and MGO

Raman spectra also offer some useful information. Fig. 5 shows the Raman spectra of the resulting GO and MGO. Two obvious peaks at $1,330$ and $1,590\text{ cm}^{-1}$ were corresponding to the D and G bands, respectively. The D band derives from the vibration of sp^3 defective or disordered carbon atoms in the graphitic structure, while the G band is associated with the first order bond stretching of sp^2 carbon atoms and provided information about the in-plane vibration of sp^2 -bonded carbon atoms [20,23]. The intensity ratio of D to G bands (I_D/I_G) of MGO increased from 0.9 of GO to 1.2, implying an increase in the defects and edges of the GO matrix with the introduction of Fe_3O_4 nanoparticles into the sp^2 -bonded orbital of GO.

3.1.5. VSM analysis

The magnetization property of Fe_3O_4 and MGO composite is investigated at room temperature by measuring the magnetization curve, as shown in Fig. 6. The saturation magnetizations of Fe_3O_4 and MGO were 80.0 , $50.0\text{ emu}\cdot\text{g}^{-1}$, respectively, indicating that MGO composite had a high magnetism and could be easily separated from solution by external magnetic field, because saturation magnetization of $16.3\text{ emu}\cdot\text{g}^{-1}$ was sufficient for magnetic separation with a conventional magnet [24].

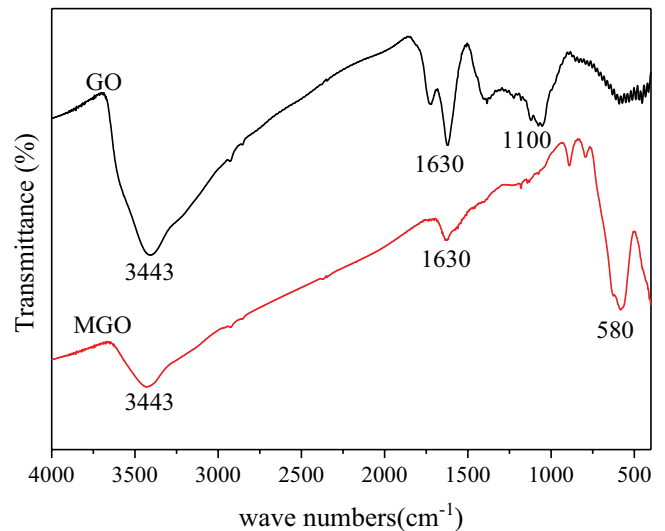


Fig. 4. FT-IR characterization of GO and MGO.

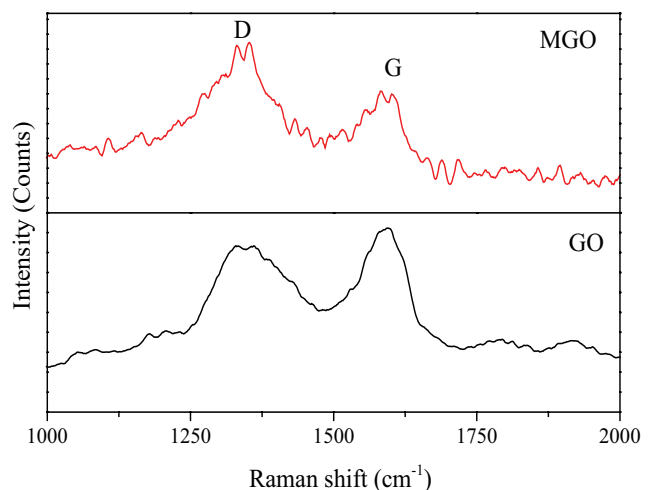


Fig. 5. Raman spectra of GO and MGO.

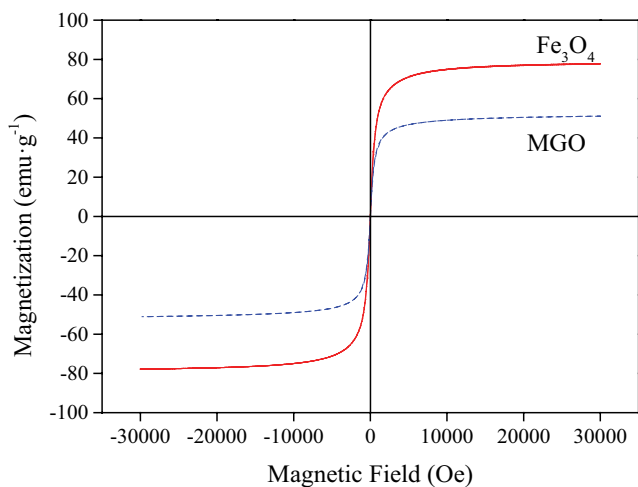


Fig. 6. Magnetization curves of Fe_3O_4 and MGO (293 K).

3.1.6. XPS of MGO

The chemical composition and relative content of the surface element for environmental material are important to the effects in application of wastewater treatment [25]. Therefore, to explore the characteristics of the MGO surface, the XPS spectra analysis of O 1s, Fe 2p, before and after MB adsorption are carried out in Fig. 7. The C 1s spectra peak of MGO could be resolved into three component peak appeared at 283.7, 285.8, and 288.1 eV shown in Fig. 7(a), corresponding to C–C, C–O, and C=O groups, respectively, which was consistent with the results of FT-IR. The peaks of Fe 2p at 709.6 and 722.5 eV demonstrated the Fe_3O_4 was successfully coated on GO, shown in Fig. 7(b), the results were similar to the previous report [26].

XPS is applied to further investigate the groups attached to the surface of adsorbent. Fig. 7(c) displays the survey spectra of MGO before and after its reaction with MB. The full survey scan of XPS spectra showed the peaks at binding energies of about 283.7, 529.1, and 709.4 eV, which corresponded to C 1s, O 1s, and Fe 2p, respectively. After the adsorption, a new binding peak of N 1s appeared at 398.6 eV, indicating that the MB molecules were adsorbed by MGO [27].

3.2. Adsorption study

3.2.1. Effects of adsorbent dose

The adsorbent dosage is one of the important factors to evaluate the adsorption properties. Therefore, different masses of MGO were added to 10 mL MB solution ($100 \text{ mg}\cdot\text{L}^{-1}$) at 303 K for 12 h, and the effect of adsorbent dose on adsorption is shown in Fig. 8.

It was seen that the removal efficiency (p) of MB increased from 13.7% to 92.3% which was due to the increase of adsorption active sites at the adsorbent surface with increasing adsorbent dosage. And the values of q_e decreased from 68.5 to 46.1 $\text{mg}\cdot\text{g}^{-1}$ with the increase of adsorbent dosage because the amount of MB adsorbed onto unit weight of adsorbent reduced with the increase of adsorbent mass, thus causing a decrease in q_e values. In next study, 1.0 $\text{g}\cdot\text{L}^{-1}$ of adsorbent dose was chosen.

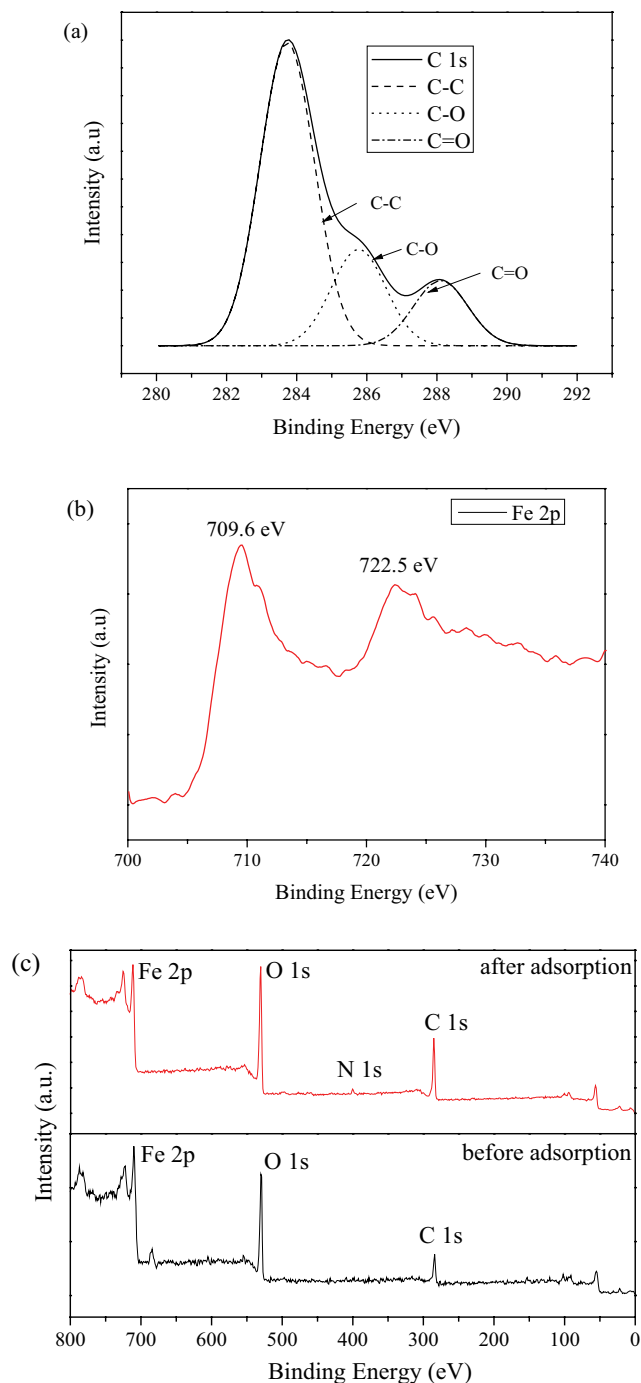


Fig. 7. XPS spectra of MGO. (a) O 1s spectra; (b) Fe 2p spectra; (c) spectra of MGO before and after MB adsorption.

3.2.2. Effects of solution pH

Solution pH often plays an important role in adsorption process as pH can affect the existing form of adsorbate and surface property of adsorbent. Values of q_e at various solution pH are illustrated in Fig. 9. It is observed from Fig. 9 that values of q_e increased rapidly under the acidic condition and rose slowly under the alkaline condition, the maximum adsorption amount of MB on MGO was $66.24 \text{ mg}\cdot\text{g}^{-1}$

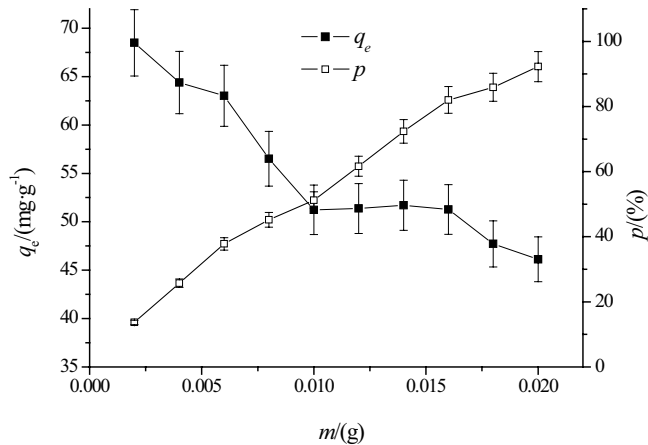


Fig. 8. Effect of adsorbent dose on MB adsorption ($C_0 = 100 \text{ mg}\cdot\text{L}^{-1}$, $t = 720 \text{ min}$, $T = 303 \text{ K}$).

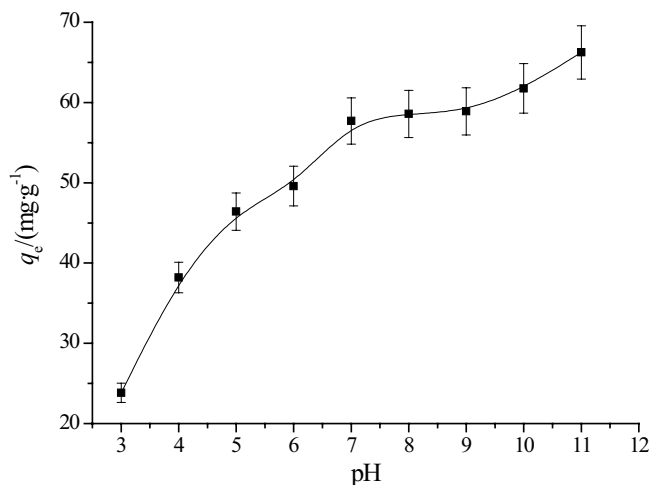


Fig. 9. Effect of solution pH on MB adsorption ($C_0 = 100 \text{ mg}\cdot\text{L}^{-1}$, $t = 720 \text{ min}$, $T = 303 \text{ K}$).

occurred at pH 11. With the increasing pH values, the adsorption of MB on MGO tended to increase, which could be explained by the increasing electrostatic interaction between the cationic dye adsorbate species and positively charged adsorbent surfaces. The point of zero charge, pH_{pzc} of MGO in aqueous solution was 6.59. When the solution pH was above 6.59, the surface of MGO was negatively charged due to these oxygen-containing functional groups (hydroxyl and carboxyl groups) with electronegative, which could exert a strong electrostatic attraction and made the adsorption capacity of MGO to increase significantly. Also lower adsorption at lower pH was due to the presence of excess H^+ ions in the solution and the protonation of MGO might compete with MB cationic dyes. However, when the solution pH value was 3.0, the adsorption capacity could still reach $23.8 \text{ mg}\cdot\text{g}^{-1}$, which might be attributed to other actions, such as π - π stacking interaction between the adsorbent and adsorbate. So the high solution pH was favorable for the adsorption for cationic MB. Because of the steady pH range between 7 and 9, pH would be adjusted to 9 in the

next experiments. The similar behaviors were also observed for MB dye adsorption onto modified nanoporous magnetic cellulose-chitosan microspheres [25], and onto biochar from pyrolysis of wheat straw [28].

3.2.3. Effects of NaCl and CaCl_2

In natural water, there exist many cationic and anionic ions such as K^+ , Na^+ , Mg^{2+} , Ca^{2+} , Cl^- , HCO_3^- , SO_4^{2-} which might compete with MB for the active adsorption sites. Therefore, it is necessary to investigate the potential influence of co-existing ions on MB adsorption. The effects of various NaCl and CaCl_2 concentration on MB adsorption are performed and the results are shown in Fig. 10. The increase in the salt concentration from 0 to $0.06 \text{ mol}\cdot\text{L}^{-1}$ resulted in a decrease of values of q_e from 58.9 to 43.3, and $22.0 \text{ mg}\cdot\text{L}^{-1}$ for NaCl and CaCl_2 , respectively. This trend indicated that there was a negative effect of co-existing ions on the adsorption of MB by MGO, which could be attributed to the competitive effect between MB ions and cations from the salt for the sites available for the adsorption process. Furthermore, the effect of Ca^{2+} is more serious than Na^+ in the same mole concentration as Ca^{2+} has more contribution to ionic strength and more positive charge than Na^+ [26]. It can be referred that electrostatic attraction may be a main mechanism according to the results obtained from effects of solution pH and salt concentration.

3.2.4. Kinetic study

Effect of contacting time is also important to study and the results are shown at various temperatures in Fig. 11. It was obviously found that values of q_e rapidly increased during the initial stage and then increased at a slow speed. It was also seen that there was higher adsorption quantity at higher temperature.

In order to explore the adsorption rate and mechanism, the pseudo-first-order kinetic model, pseudo-second-order kinetic model and Elovich equation were used to predict the adsorption process. The pseudo-first-order kinetic model

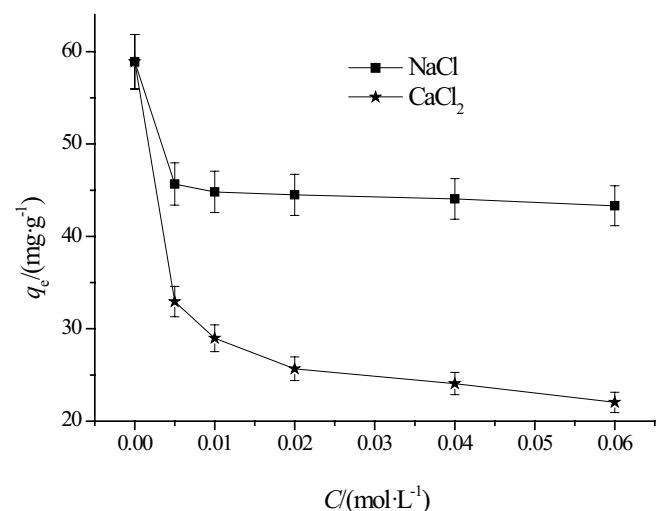


Fig. 10. Effect of NaCl and CaCl_2 concentration on MB adsorption ($C_0 = 100 \text{ mg}\cdot\text{L}^{-1}$, $\text{pH} = 9$, $t = 720 \text{ min}$, $T = 303 \text{ K}$).

assumes that the adsorption rate is proportional to the available number of adsorption site, while the pseudo-second-order model is based on the assumption that the rate limiting step may be chemical adsorption involving forces through sharing or electronic exchange between MGO and MB [29–31]. Elovich model is used to describe the heterogeneous adsorption of the ion exchange system [32]. The expressions of three kinetic models were following:

Pseudo-first-order kinetic model:

$$q_t = q_e (1 - e^{-k_1 t}) \quad (3)$$

Pseudo-second-order kinetic model:

$$q_t = \frac{k_2 q_e^2 t}{1 + k_2 q_e t} \quad (4)$$

Elovich equation:

$$q_t = \frac{\ln(\alpha\beta)}{\beta} + \frac{\ln t}{\beta} \quad (5)$$

where q_t and q_e represent the adsorption quantity ($\text{mg}\cdot\text{g}^{-1}$) at time t and at equilibrium ($\text{mg}\cdot\text{g}^{-1}$); k_1 (min^{-1}) and k_2 ($\text{g}\cdot\text{mg}^{-1}\cdot\text{min}^{-1}$) are the rate constants of pseudo-first-order and pseudo-second-order kinetic models, respectively; α is the initial adsorption rate constant ($\text{mg}\cdot\text{g}^{-1}\cdot\text{min}^{-1}$) and the parameter β is related to the extent of surface coverage and activation energy for chemisorption ($\text{g}\cdot\text{mg}^{-1}$).

The parameters of the kinetic models, calculated $q_{e(\text{theo})}$, determined coefficients (R^2) and the sum of squares of the errors (SSE) are listed in Table 1 using nonlinear regressive

Table 1
Parameters of kinetic models for MB adsorption

| Pseudo-first-order kinetic model | | | | | |
|-----------------------------------|---------------------------------------------------|----------------------------------------------------|----------------------|-------|------|
| T/K | $q_{e(\text{exp})}/(\text{mg}\cdot\text{g}^{-1})$ | $q_{e(\text{theo})}/(\text{mg}\cdot\text{g}^{-1})$ | $k_1 \times 10^{-2}$ | R^2 | SSE |
| 293 | 46.1 | 38.3 ± 2.0 | 1.94 ± 0.41 | 0.789 | 217 |
| 303 | 53 | 48.6 ± 2.1 | 1.71 ± 0.29 | 0.865 | 232 |
| 313 | 62.7 | 56.2 ± 2.3 | 2.01 ± 0.35 | 0.861 | 314 |
| Pseudo-second-order kinetic model | | | | | |
| T/K | $q_{e(\text{exp})}/(\text{mg}\cdot\text{g}^{-1})$ | $q_{e(\text{theo})}/(\text{mg}\cdot\text{g}^{-1})$ | $k_2 \times 10^{-4}$ | R^2 | SSE |
| 293 | 46.1 | 42.5 ± 1.7 | 6.34 ± 1.38 | 0.916 | 86.9 |
| 303 | 53.0 | 54.0 ± 1.6 | 4.45 ± 0.70 | 0.958 | 71.7 |
| 313 | 62.7 | 62.4 ± 1.7 | 4.39 ± 0.65 | 0.962 | 85.8 |
| Elovich equation | | | | | |
| T/K | $q_{e(\text{exp})}/(\text{mg}\cdot\text{g}^{-1})$ | α | β | R^2 | SSE |
| 293 | 46.1 | 3.99 ± 1.37 | 0.273 ± 0.139 | | |
| 303 | 53.0 | 4.28 ± 1.32 | 0.264 ± 0.107 | 0.991 | 14.9 |
| 313 | 62.7 | 5.61 ± 1.22 | 0.244 ± 0.093 | 0.994 | 12.8 |

Note: $\text{SSE} = \sum(q - q_e)^2$, q and q_e are the experimental value and calculated value according to the model, respectively.

analysis, and the fitted curves are also shown in Fig. 11. It was found that the fitted curves from Elovich equation were closest to experimental points. So Elovich equation was best to describe the kinetic process with highest R^2 and minimum SSE (Table 1). In addition, the $q_{e(\text{theo})}$ values of the pseudo-second-order kinetic model were very closer to the measured $q_{e(\text{exp})}$ than the pseudo-first-order kinetic model, which turned out that the adsorption system was a chemical process. Therefore, it was concluded that there be chemical action during adsorption process.

3.2.5. Adsorption equilibrium study

The equilibrium adsorption isotherm is fundamentally important in the surface properties of MGO, and expresses the adsorption behavior and the design of adsorption systems. The experimental equilibrium data of MB adsorption onto MGO at pH 9 are presented in Fig. 12. With the increasing of MB concentration, values of q increased rapidly and became slow, and finally reached equilibrium. Furthermore, it could also be seen from the result that the adsorption capacities of MGO for MB increased with the increasing temperature from 293 to 313 K. So it was in favor of MB adsorption at high temperature and the process was an endothermic reaction.

In the present study, the Langmuir model, Freundlich model, and Koble–Corrigan model were used to analyze the experimental data. The Langmuir model assumes that adsorbed molecules are organized as a monolayer and all sites are energetically equivalent and there is no interaction between adsorbed molecules. The Freundlich isotherm is based on multilayer adsorption and a non-ideal adsorption method for heterogeneous surface suggesting that adsorption energy exponentially decreases on completion of the adsorption center of an adsorbent [33]. The Koble–Corrigan isotherm is a three-parameter model, a combination of Langmuir and Freundlich isotherm models. When B is close to 0, the equation is converted to Freundlich isotherm. When n is close to 1, the Koble–Corrigan isotherm is approached

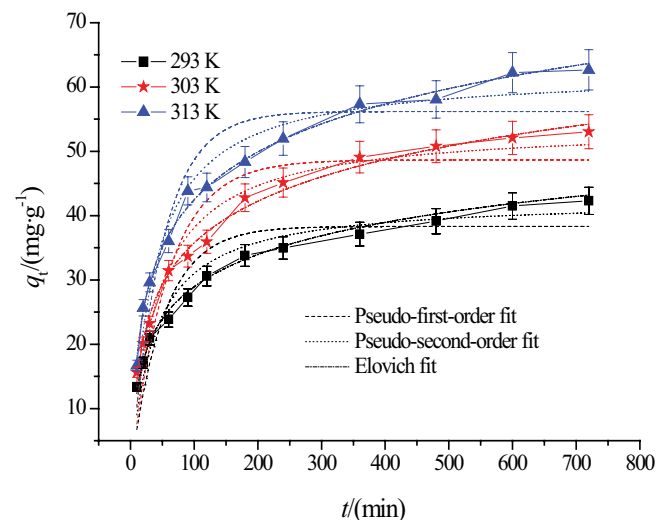


Fig. 11. Effect of contact time on MB adsorption ($C_0 = 100 \text{ mg}\cdot\text{L}^{-1}$, pH = 9).

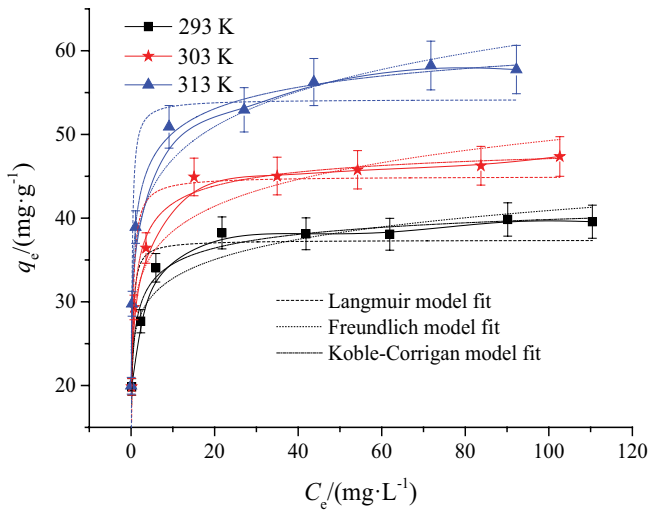


Fig. 12. Adsorption isotherms and fitted curves of MB adsorption onto MGO (pH = 9, $t = 360$ min).

to Langmuir isotherm. The three isotherm models can be expressed as follows [34]:

The equation of Langmuir isotherm:

$$q_e = \frac{q_m K_L C_e}{1 + K_L C_e} \quad (6)$$

The Freundlich isotherm equation:

$$q_e = K_F C_e^{1/n} \quad (7)$$

The Koble–Corrigan isotherm:

$$q_e = \frac{A C_e^n}{1 + B C_e^n} \quad (8)$$

where q_m is the maximum adsorption capacity ($\text{mg}\cdot\text{g}^{-1}$), K_L is a constant related to the affinity of the binding sites and energy of adsorption ($\text{L}\cdot\text{mg}^{-1}$); K_F is the constant of the Freundlich isotherm, $1/n$ is the constant which is related to the adsorption capacity and the adsorption intensity; A , B , and n are the Koble–Corrigan parameters.

All parameters of three models are displayed in Table 2 using nonlinear regression and the fitted curves are also shown in Fig. 12. It was obvious that the values of R^2 obtained from Koble–Corrigan model were highest and the values of SSE were lowest, while the fitted curves from Koble–Corrigan model were closest to experimental points. So the adsorption processes were in accordance with the Koble–Corrigan model. Moreover, the values of n from Koble–Corrigan model were between 0 and 1, and were all closer to 0, which indicated that the Koble–Corrigan model was closer to Freundlich model. So it was implied that the adsorption process may be of the multi-molecular layer adsorption with heterogeneous surface. And values of K_F from Freundlich model became larger with the increase of temperature, which also indicated that the process was endothermic.

Table 2
Parameters of adsorption isotherm models for MB adsorption

| Langmuir | | | | | |
|----------------|---------------------------------------------------|----------------------------------------------------|-------------------------------------|-------|------|
| T/K | $q_{m(\text{exp})}/(\text{mg}\cdot\text{g}^{-1})$ | $q_{m(\text{theo})}/(\text{mg}\cdot\text{g}^{-1})$ | $K_L/(\text{L}\cdot\text{mg}^{-1})$ | R^2 | SSE |
| 293 | 39.8 | 37.4 ± 1.4 | 5.47 ± 2.07 | 0.764 | 72 |
| 303 | 47.4 | 45.0 ± 1.4 | 3.85 ± 1.01 | 0.888 | 67.5 |
| 313 | 58.2 | 54.2 ± 2.9 | 6.29 ± 2.85 | 0.789 | 264 |
| Freundlich | | | | | |
| T/K | $q_{m(\text{exp})}/(\text{mg}\cdot\text{g}^{-1})$ | $K_F/(\text{mg}\cdot\text{g}^{-1})$ | $1/n(\times 10^{-2})$ | R^2 | SSE |
| 293 | 39.8 | 26.3 ± 1.3 | 9.60 ± 1.30 | 0.911 | 27.2 |
| 303 | 47.4 | 30.0 ± 1.6 | 10.8 ± 1.5 | 0.908 | 55.8 |
| 313 | 58.2 | 36.1 ± 1.4 | 11.4 ± 1.1 | 0.959 | 50.6 |
| Koble–Corrigan | | | | | |
| T/K | A | B | n | R^2 | SSE |
| 293 | 63.8 ± 11.4 | 1.41 ± 0.37 | 0.355 ± 0.086 | 0.964 | 9.20 |
| 303 | 82.4 ± 8.7 | 1.63 ± 0.23 | 0.469 ± 0.060 | 0.989 | 5.78 |
| 313 | 87.7 ± 8.1 | 1.27 ± 0.18 | 0.323 ± 0.031 | 0.996 | 4.54 |

3.2.6. Thermodynamic analysis

To explain if the adsorption of MB on the MGO composites is endothermic or exothermic and spontaneous, the thermodynamic parameters including enthalpy change (ΔH°), Gibbs free energy change (ΔG°) and entropy change (ΔS°) were determined using the temperature-dependent adsorption results using the following equations:

$$K_c = \frac{C_{\text{ad,e}}}{C_e} \quad (9)$$

$$\Delta G^\circ = -RT \ln K_c \quad (10)$$

$$\Delta G^\circ = \Delta H^\circ - T\Delta S^\circ \quad (11)$$

where K_c is the distribution coefficient of the adsorption, $C_{\text{ad,e}}$ is the concentration of MB on the adsorbent at equilibrium ($\text{mg}\cdot\text{L}^{-1}$), R ($8.314 \text{ J}\cdot\text{mol}^{-1}\cdot\text{K}^{-1}$) is the ideal gas constant, T is temperature (K).

The thermodynamic parameters calculated by the above equations are listed in Table 3. The negative values of ΔG° indicated that the adsorption processes were spontaneous. In addition, values of ΔG° decreased with an increasing temperature suggested that the adsorption be endothermic. The positive value of ΔH° also showed the endothermic reaction and the value was more than $40 \text{ kJ}\cdot\text{mol}^{-1}$, proving the reaction contained the chemical process. Besides, the positive value of ΔS° demonstrated the increasing randomness at the solid–solution interface during MB adsorption onto MGO [35,36]. The value of E_a was $13.0 \text{ kJ}\cdot\text{mol}^{-1}$, between 5 and $40 \text{ kJ}\cdot\text{mol}^{-1}$, indicating that there was physical action during adsorption process. In summary, the adsorption was the process both with chemical and physical reaction. The thermodynamic parameters indicated that the adsorption was spontaneous and endothermic.

Table 3
Thermodynamic parameters of MB adsorption onto MGO

| E_a /(KJ·mol ⁻¹) | ΔH /(KJ·mol ⁻¹) | ΔS /(J·(mol·K) ⁻¹) | ΔG /(KJ·mol ⁻¹) | | |
|--------------------------------|-------------------------------------|----------------------------------------|-------------------------------------|-------|-------|
| | | | 293 K | 303 K | 313 K |
| 13.0 | 54.3 | 223 | -11.7 | -12.1 | -16.1 |

3.2.7. Secondary adsorption for congo red

Reuse of spent adsorbent can make the adsorption process economical [37–39]. In this study, the spent or exhausted adsorbent (MB-loaded MGO) was used in second adsorption to another pollutant, CR. The adsorption quantity of CR onto MGO and MB-loaded MGO is shown in Fig. 13. It can be seen from Fig. 13 that the adsorption capacities of MB-loaded MGO for CR were significantly greater than the direct adsorption under the same conditions, indicating that the MGO surface was negatively charged and it was hard to adsorb anionic dyes such as CR. MB-loaded MGO had the better adsorption capacity toward CR. Besides, salinity was favorable for the adsorption processes as the value of q_e could improve approximately 40.7% with no salt and 18.1% with salt, respectively. When the salt existed in the solution, it was possible to decrease the repulsive forces and thus increase the anionic exchange capacity. So the MB-loaded MGO can be used to remove CR from aqueous solution with a higher salt concentration. Generally, MB bound on MGO can act with CR through Van der Waals forces and hydrogen bonding as surface property of MGO changed after MB adsorption. This was similar to adsorbents modified by surface activated agents to enhance adsorption capacity toward anionic pollutants [40,41]. The comparison of MB and CR adsorption capacity by MGO and other adsorbents was listed in Table 4. It can be referred that MGO has the medium-level adsorption capacity for MB, whereas MB-loaded MGO has superior capacity for CR from solution.

3.2.8. Adsorption mechanism

The results of the FT-IR, XPS, and adsorption tests show that the oxygen-containing functional groups play an

important role during the adsorption process. The reaction mechanisms were formulated as the following equations [20]:



where R is the MGO.

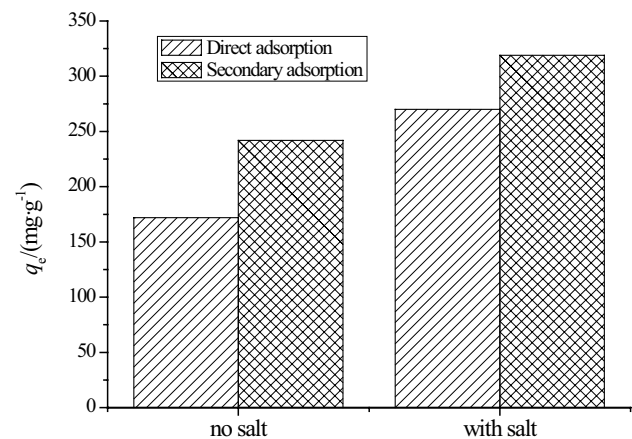


Fig. 13. Direct and secondary adsorption for Congo red ($C_0 = 500 \text{ mg}\cdot\text{L}^{-1}$, $\text{pH} = 6.06$, $t = 360 \text{ min}$, $T = 303 \text{ K}$).

Table 4
Comparison of adsorption capacity with various adsorbents for MB and CR

| Adsorbents | Target dye | Adsorption capacity (mg·g ⁻¹) | Ref. |
|---------------------------------------------------------------|------------|-------------------------------------------|---------------|
| Wheat straw biochar | MB | 62.5 | [42] |
| Carbon-doped graphitic carbon nitride | MB | 57.9 | [43] |
| Congo red functionalized $\text{Fe}_3\text{O}_4/\text{SiO}_2$ | MB | 31.4 | [44] |
| β -Cyclodextrin modified magnetic graphene oxide | MB | 94.0 | [45] |
| Magnetic graphene oxide | MB | 62.7 | Present study |
| Acid-treated pine cone | CR | 40.2 | [46] |
| Polyethyleneimine-modified wheat straw | CR | 89.7 | [47] |
| La_2O_3 -doped TiO_2 nanotubes | CR | 131 | [48] |
| Magnesium oxide (MgO)-graphene oxide | CR | 237 | [49] |
| MB-loaded magnetic graphene oxide | CR | 319 | Present study |

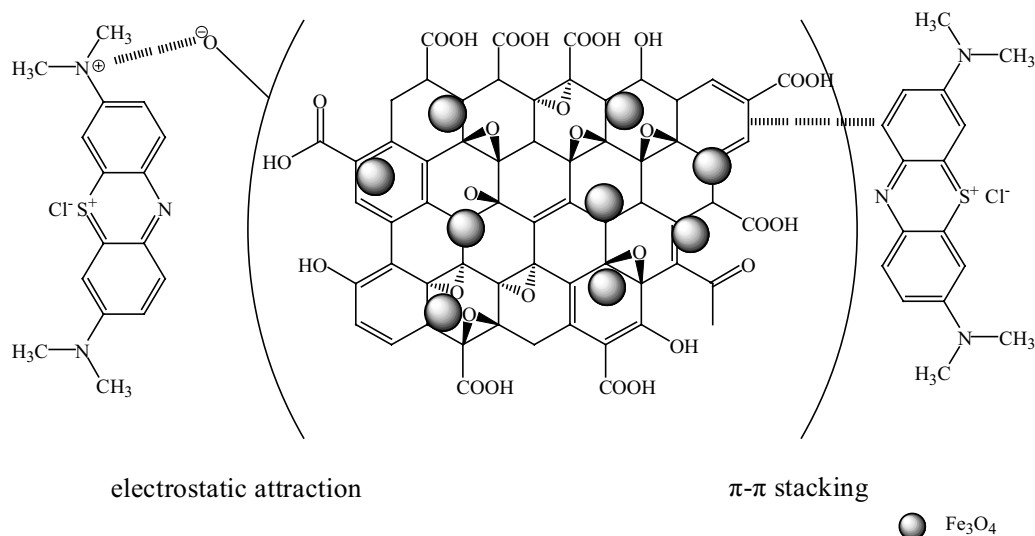


Fig. 14. Schematic illustration of adsorption mechanism between the MGO and MB.

The reactions show that the more OH^- corresponds, the more chance to react with H^+ under high solution pH, demonstrating electrostatic attraction as the main mechanism for cationic MB with positive charge. In addition, the π - π stacking is a special spatial arrangement of aromatic compounds, referring to a weak interaction that often occurs between aromatic rings, so the π - π stacking reaction is likely to occur between the MGO and MB for their abundant aromatic rings. In summary, the main possible interaction between the MGO and MB are illustrated in Fig. 14.

4. Conclusion

In the present study, MGO composites were prepared and characterized. There were good adsorption capacity toward MB and the adsorbent was easily separated from solution by external magnet, which could greatly simplify the separation and reduce the energy consumption. The optimal solution pH for adsorption was pH 9 and the existence of salts was disadvantage of MB adsorption. Kinetics data were best fitted by Elovich equation while the equilibrium data were best fitted by Koble–Corrigan model. The MB adsorption processes were spontaneous and endothermic in nature. And the secondary adsorption with salt for CR was practical and meaningful. The adsorption mechanism can be attributed to the electrostatic interaction and π - π stacking.

References

- [1] Y.C. Qi, M.L. Yang, W.H. Xu, S. He, Y. Men, Natural polysaccharides-modified graphene oxide for adsorption of organic dyes from aqueous solutions, *J. Colloid Interface Sci.*, 486 (2017) 84–96.
- [2] P.F. Wang, M.H. Cao, C. Wang, Y.H. Ao, J. Hou, J. Qian, Kinetics and thermodynamics of adsorption of methylene blue by a magnetic graphene-carbon nanotube composite, *Appl. Surf. Sci.*, 290 (2014) 116–124.
- [3] Y.L. Luo, R.X. Bai, F. Xu, Y.S. Chen, H. Li, S.S. Dai, W.B. Ma, Novel multiwalled carbon nanotube grafted with polyethylene glycol-block-polystyrene nano-hybrids: ATRP synthesis and detection of benzene vapor, *J. Mater. Sci.*, 51 (2016) 1363–1375.
- [4] R. Rostamian, H. Behnejad, Insights into doxycycline adsorption onto graphene nanosheet: a combined quantum mechanics, thermodynamics, and kinetic study, *Environ. Sci. Pollut. Res.*, 25 (2018) 2528–2537.
- [5] F. Yu, Y. Li, S. Han, J. Ma, Adsorptive removal of antibiotics from aqueous solution using carbon materials, *Chemosphere*, 153 (2016) 365–385.
- [6] Y.J. Yao, F.F. Xu, M. Chen, Z.X. Xu, Z.W. Zhu, Adsorption behavior of methylene blue on carbon nanotubes, *Bioresour. Technol.*, 101 (2010) 3040–3046.
- [7] T. Zhou, W.Z. Lu, L.F. Liu, H.M. Zhu, Y.B. Jiao, S.S. Zhang, R.P. Han, Effective adsorption of light green anionic dye from solution by CPB modified peanut in column mode, *J. Mol. Liq.*, 211 (2015) 909–914.
- [8] R. Ianos, C. Păcurariu, G. Mihoc, Magnetite/carbon nanocomposites prepared by an innovative combustion synthesis technique-excellent adsorbent materials, *Ceram. Int.*, 40 (2014) 13649–13657.
- [9] X.W. Chen, X. Hai, J.H. Wang, Graphene/graphene oxide and their derivatives in the separation/isolation and preconcentration of protein species: a review, *Anal. Chim. Acta*, 922 (2016) 1–10.
- [10] W. Gao, M. Majumder, L.B. Alemany, T.N. Narayanan, M.A. Ibarra, B.K. Pradhan, P.M. Ajayan, Engineered graphite oxide materials for application in water purification, *ACS Appl. Mater. Interfaces*, 3 (2011) 1821–1826.
- [11] J. Molina, F. Cases, L.M. Moretto, Graphene-based materials for the electrochemical determination of hazardous ions, *Anal. Chim. Acta*, 946 (2016) 9–39.
- [12] S.F. Wang, X. Li, Y.G. Liu, C. Zhang, X.F. Tan, G.M. Zeng, B. Song, L.H. Jiang, Nitrogen-containing amino compounds functionalized graphene oxide: synthesis, characterization and application for the removal of pollutants from wastewater: a review, *J. Hazard. Mater.*, 342 (2018) 177–191.
- [13] S.J. Liu, S. Li, H.X. Zhang, L.P. Wu, L. Sun, J.G. Ma, Removal of uranium(VI) from aqueous solution using graphene oxide and its amine-functionalized composite, *J. Radioanal. Nucl. Chem.*, 309 (2016) 607–614.
- [14] D. Konios, M.M. Stylianakis, E. Stratakis, E. Kymakis, Dispersion behaviour of graphene oxide and reduced graphene oxide, *J. Colloid Interface Sci.*, 430 (2014) 108–112.
- [15] F. Wang, C. Guo, H.Z. Liu, C.Z. Liu, Immobilization of *Pycnoporus sanguineus* laccase by metal affinity adsorption on magnetic chelator particles, *J. Chem. Technol. Biotechnol.*, 83 (2008) 97–104.

- [16] J.F. Lin, C.C. Tsai, M.Z. Lee, Linear birefringence and dichroism in citric acid coated Fe_3O_4 magnetic nanoparticles, *J. Magn. Magn. Mater.*, 372 (2014) 147–158.
- [17] B. Jiang, L. Lian, Y. Xing, N.N. Zhang, Y.T. Chen, P. Lu, D.Y. Zhang, Advances of magnetic nanoparticles in environmental application: environmental remediation and (bio) sensors as case studies, *Environ. Sci. Pollut. Res.*, 25 (2018) 30863–30879.
- [18] Q. Wu, C. Feng, C. Wang, Z. Wang, A facile one-pot solvothermal method to produce superparamagnetic graphene- Fe_3O_4 nanocomposite and its application in the removal of dye from aqueous solution, *Colloids Surf., B*, 101 (2013) 210–214.
- [19] C. Wang, C. Feng, Y.J. Gao, X.X. Ma, Q.H. Wu, Z. Wang, Preparation of a graphene-based magnetic nanocomposite for the removal of an organic dye from aqueous solution, *Chem. Eng. J.*, 173 (2011) 92–97.
- [20] Y.F. Guo, J. Deng, J.Y. Zhu, X.J. Zhou, R.B. Bai, Removal of mercury(II) and methylene blue from a wastewater environment with magnetic graphene oxide: adsorption kinetics, isotherms and mechanism, *RSC Adv.*, 6 (2016) 82523–82536.
- [21] J.W. Zhang, M.S. Azam, C. Shi, J. Huang, B. Yan, Q.X. Liu, H.B. Zeng, Poly(acrylic acid) functionalized magnetic graphene oxide nanocomposite removal of methylene blue, *RSC Adv.*, 5 (2015) 32272–32282.
- [22] Y.Y. Chen, S.H. Yu, H.F. Jiang, Q.Z. Yao, S.Q. Fu, G.T. Zhou, Performance and mechanism of simultaneous removal of Cd(II) and Congo red from aqueous solution by hierarchical vaterite spherulites, *Appl. Surf. Sci.*, 444 (2018) 224–234.
- [23] B.K. Choi, W.K. Choi, S.J. Park, M.K. Seo, One-pot synthesis of ag- TiO_2 /nitrogen-doped graphene oxide nanocomposites and its photocatalytic degradation of methylene blue, *J. Nanosci. Nanotechnol.*, 18 (2018) 6075–6080.
- [24] M.F. Li, Y.G. Liu, G.M. Zeng, S.B. Liu, X.J. Hu, D. Shu, L.H. Jiang, X.F. Tan, X.X. Cai, Z.L. Yan, Tetracycline adsorbed onto nitrilotriacetic acid-functionalized magnetic graphene oxide: Influencing factors and uptake mechanism, *J. Colloid Interface Sci.*, 485 (2017) 269–279.
- [25] S. Peng, Y. Liu, Z.Y. Xue, W.Y. Yin, X.C. Liang, M. Li, J. Chang, Modified nanoporous magnetic cellulose-chitosan microspheres for efficient removal of Pb(II) and methylene blue from aqueous solution, *Cellulose*, 24 (2017) 4793–4806.
- [26] J.H. Deng, X.R. Zhang, G.M. Zeng, J.L. Gong, Q.Y. Niu, J. Liang, Simultaneous removal of Cd(II) and ionic dyes from aqueous solution using magnetic graphene oxide nanocomposite as an adsorbent, *Chem. Eng. J.*, 226 (2013) 189–200.
- [27] Y. Yan, J. Li, F.B. Kong, K.K. Jia, S.Y. He, B.R. Wang, L-Lysine-grafted graphene oxide as an effective adsorbent for the removal of methylene blue and metal ions, *Beilstein J. Nanotechnol.*, 8 (2017) 2680–2688.
- [28] Y.L. Liu, X.R. Zhao, J.L. Li, D. Ma, R.P. Han, Characterization of bio-char from pyrolysis of wheat straw and its evaluation on methylene blue adsorption, *Desal. Wat. Treat.*, 46 (2012) 115–123.
- [29] J.Y. Song, W.H. Zou, Y.Y. Bian, F.Y. Su, R.P. Han, Adsorption characteristics of methylene blue by peanut husk in batch and column mode, *Desalination*, 265 (2011) 119–125.
- [30] F. Gunduz, B. Bayrak, Biosorption of malachite green from an aqueous solution using pomegranate peel: equilibrium modelling, kinetic and thermodynamic studies, *J. Mol. Liq.*, 243 (2017) 790–798.
- [31] M.I. Konggidinata, B. Chao, Q.Y. Lian, R. Subramaniam, M. Zappi, D.D. Gang, Equilibrium, kinetic and thermodynamic studies for adsorption of BTEX onto Ordered Mesoporous Carbon (OMC), *J. Hazard. Mater.*, 336 (2017) 249–259.
- [32] T. Maneerung, J. Liew, Y. Dai, S. Kawi, C. Chong, C.H. Wang, Activated carbon derived from carbon residue from biomass gasification and its application for dye adsorption: kinetics, isotherms and thermodynamic studies, *Bioresour. Technol.*, 200 (2016) 350–359.
- [33] H.Y. Ge, C.C. Wang, S.S. Liu, Z. Huang, Synthesis of citric acid functionalized magnetic graphene oxide coated corn straw for methylene blue adsorption, *Bioresour. Technol.*, 221 (2016) 419–429.
- [34] Y.C. Rong, H. Li, L.H. Xiao, Q. Wang, Y.Y. Hu, S.S. Zhang, R.P. Han, Adsorption of malachite green dye from solution by magnetic activated carbon in batch mode, *Desal. Wat. Treat.*, 106 (2018) 273–284.
- [35] W. Konicki, M. Aleksandrak, D. Moszyński, E. Mijowska, Adsorption of anionic azo-dyes from aqueous solutions onto graphene oxide: equilibrium, kinetic and thermodynamic studies, *J. Colloid Interface Sci.*, 496 (2017) 188–200.
- [36] M.Y. Han, Q. Wang, H. Li, L.Y. Fang, R.P. Han, Removal of methyl orange from aqueous solutions by polydopamine mediated surface functionalization of Fe_3O_4 in batch mode, *Desal. Wat. Treat.*, 115 (2018) 271–280.
- [37] R.P. Han, Y. Wang, Q. Sun, L.L. Wang, J.Y. Song, X.T. He, C.C. Dou, Malachite green adsorption onto natural zeolite and reuse by microwave irradiation, *J. Hazard. Mater.*, 175 (2010) 1056–1061.
- [38] Y.B. Jiao, D.L. Han, Y.C. Rong, L.Y. Fang, Y.L. Liu, R.P. Han, Characterization of pine-sawdust pyrolytic char activated by phosphoric acid through microwave irradiation and adsorption property toward CDNB in batch mode, *Desal. Wat. Treat.*, 77 (2017) 247–255.
- [39] S. Sadaf, H.N. Bhatti, Evaluation of peanut husk as a novel, low cost biosorbent for the removal of Indosol Orange RSN dye from aqueous solutions batch and fixed bed studies, *Clean Technol. Environ. Policy*, 16 (2014) 527–544.
- [40] R.D. Zhang, J.H. Zhang, X.N. Zhang, C.C. Dou, R.P. Han, Adsorption of Congo red from aqueous solutions using cationic surfactant modified wheat straw in batch mode: Kinetic and equilibrium study, *J. Taiwan Inst. Chem. Eng.*, 45 (2014) 2578–2583.
- [41] B.L. Zhao, W. Xiao, Y. Shang, H.M. Zhu, R.P. Han, Adsorption of light green anionic dye using cationic surfactant-modified peanut husk in batch mode, *Arabian J. Chem.*, 10 (2017) S3595–S3602.
- [42] G.T. Li, W.Y. Zhu, C.Y. Zhang, S. Zhang, L.L. Liu, L.F. Zhu, W.G. Zhao, Effect of a magnetic field on the adsorptive removal of methylene blue onto wheat straw biochar, *Bioresour. Technol.*, 206 (2016) 16–22.
- [43] B. Ren, Y.L. Xu, L.H. Zhang, Z.F. Liu, Carbon-doped graphitic carbon nitride as environment-benign adsorbent for methylene blue adsorption: kinetics, isotherm and thermodynamics study, *J. Taiwan Inst. Chem. Eng.*, 88 (2018) 114–120.
- [44] Y.M. Dai, J.Q. Zou, D.Y. Liu, L.L. Niu, L.L. Zhou, Y. Zhou, X.H. Zhang, Preparation of Congo red functionalized $\text{Fe}_3\text{O}_4@SiO_2$ nanoparticle and its application for the removal of methylene blue, *Colloids Surf., A*, 550 (2018) 90–98.
- [45] Y.X. Ma, W.J. Shao, W. Sun, Y.L. Kou, X. Li, H.P. Yang, One-step fabrication of β -cyclodextrin modified magnetic graphene oxide nanohybrids for adsorption of Pb(II), Cu(II) and methylene blue in aqueous solutions, *Appl. Surf. Sci.*, 459 (2018) 544–553.
- [46] S. Dawood, T.K. Sen, Removal of anionic dye Congo red from aqueous solution by raw pine and acid-treated pine cone powder as adsorbent: equilibrium, thermodynamic, kinetics, mechanism and process design, *Water Res.*, 46 (2012) 1933–1946.
- [47] Y. Shang, J.H. Zhang, X. Wang, R.D. Zhang, W. Xiao, S.S. Zhang, R.P. Han, Use of polyethyleneimine-modified wheat straw for adsorption of Congo red from solution in batch mode, *Desal. Wat. Treat.*, 57 (2015) 8872–8883.
- [48] H.X. Guo, J.H. Chen, W. Weng, Z.S. Zheng, D.F. Wang, Adsorption behavior of Congo red from aqueous solution on La_2O_3 -doped TiO_2 nanotubes, *J. Ind. Eng. Chem.*, 20 (2014) 3081–3088.
- [49] J. Xu, D.F. Xu, B.C. Zhu, B. Cheng, C.J. Jiang, Adsorptive removal of an anionic dye Congo red by flower-like hierarchical magnesium oxide (MgO)-graphene oxide composite microspheres, *Appl. Surf. Sci.*, 435 (2018) 1136–1142.